Supporting Information

Highly-selective light olefins production *via* photothermal Fischer–Tropsch synthesis over α/γ-Fe_2O_3-derived Fe_5C_2 under low pressure

Lizhu Song,[a] Shuxin Ouyang,*[b] Peng Li[c] and Jinhua Ye[a,d]

[a] *TJU-NIMS International Collaboration Laboratory, School of Materials Science and Engineering, Tianjin University, Tianjin 300072, P. R. China.*

[b] *Key Laboratory of Pesticide and Chemical Biology, Ministry of Education, College of Chemistry, Central China Normal University, Wuhan 430079, P. R. China.*

[c] *College of Materials Science and Technology, Jiangsu Key Laboratory of Materials and Technology for Energy Conversion, Nanjing University of Aeronautics and Astronautics, Nanjing 210016, P. R. China*

[d] *International Center for Materials Nanoarchitectonics (WPI-MANA), National Institute for Materials Science (NIMS), 1-1 Namiki, Tsukuba 305-0047, Japan*

*Corresponding author. *E-mail address:* oysx@mail.ccnu.edu.cn (S. Ouyang).

Experimental Procedures

Catalyst precursor synthesis. The method to synthesize the Fe-based catalysts for photothermal Fischer-Tropsch synthesis included the following steps: (1) 10 g $Fe(NO_3)_3 \cdot 9H_2O$ (Sinopharm Chemical Reagent Co.,Ltd, 80072718) was calcined in a tube furnace under Ar atmosphere at 500 °C for 2 h to obtain α-Fe_2O_3; (2) 0.5 g α-Fe_2O_3, 3 ml of 0.03 mol/L KNO_3 (Tianjin Guangfu Fine Chemical Research Institute, 50116) were added to 20 ml deionized water (according to the K^+ loading amounts, 0.7%); the suspension solution was stirred at 80 °C to paste, and then further dried at 70 °C for 24 h under vacuum conditions. The γ-Fe_2O_3 (Aladdin, F141282-25g) is prepared in the same steps.

Photothermal synthesis of pre-catalyst. Typically, 50 mg sample was placed in a CO atmosphere and activated for 30 min under a 300 W Xenon lamp in an enclosed-circuit reaction system (OLPCRS-3, Shanghai Boyi Scientific Instrument Co., China). After cooling to room temperature and evacuated, the reaction system was reinjected 30 kPa of air, then the sample was under irradiation again for 0, 10, 30, 50 min, respectively. Here we labeled them α(or γ)-CmAn (m, n = 0, 10, 30, 50), in which α or γ represent α(or γ)-Fe_2O_3-0.7 K^+ unless there is a special description; C and A represent the pre-catalyst was photothermally treated in CO and air, respectively; m and n signify the processing time in each atmospheric condition. In addition, γ-At means γ-Fe_2O_3-0.7 K^+ directly under irradiation in the air.

Sample characterization. The crystal structure was characterized by X-ray diffractometer (D/max-2500, Rigaku, Japan). The light adsorption properties of the catalysts were measured by Ultraviolet-visible (UV-Vis) spectroscopy (UV-2700, Shimadzu, Japan). The microstructure of the catalyst was performed on Scanning electron microscopy (SEM, Quanta FEG 250) and Transmission electron microscopy (TEM, JEM-F200). The spatial distribution of element was confirmed by energy-dispersive X-ray spectroscopy (EDS). The chemical valence state of the element was measured by Xray photoelectron spectroscopy (XPS, Escalab 250Xi, Thermo Fisher Scientific, England). The temperature of the catalyst surface was measured by a thermocouple (DT-311N). Mössbauer spectroscopy is powerful in distinguishing and quantifying the phases of Fe-based materials that are difficult to be identified by XRD. The data analysis was using the least-squares method. Spectral fits were based on Lorentzian curves. Component identification base on the isomer shift (IS), quadrupole splitting (QS), and hyperfine magnetic field (H).

Catalyst performance evaluation. The Photothermal Fischer-Tropsch synthesis was evaluated in an enclosed-circuit reaction system (OLPCRS-3, Shanghai Boyi Scientific Instrument Co., China, as presented in **Fig. S1**). 300W Xe lamp (CEL-HXF300, CEAULIGHT) was used as a photothermocatalytic light source, 50 mg of catalyst, CO: H_2 = 1: 3, 55.5 kPa. The gas composition of the products after the reaction was detected by gas chromatography (GC-2014C, Shimadzu Co., Japan) using N_2 as the carrier gas, equipped with a Paropak Q chromatographic column, a flame ionization detector (FID) and a methanizer. The components of gas products were analyzed by gas chromatography-mass spectrometry (Shimadzu, GCMS-QP2010 Ultra).

The catalytic performances were typically evaluated through the following indicators.

CO conversion rate was calculated by the following formula (S1):

$$CO_{con}(\%) = \frac{CO_0 - CO_t}{CO_0} \times 100\% \quad \text{(S1)}$$

Where CO_0 and CO_t represent the moles of CO at the beginning and at moment *t*, respectively.

Total organic carbon (TOC) products represent total hydrocarbons at moment *t* was obtained according to formula (S2), *m* represents the mass of the catalyst:

$$TOC = \frac{1}{m} \times \sum_{i=1}^{n} moles\ of\ C_i\ hydrocarbon\ \times i \quad \text{(S2)}$$

The selectivity of $C_i\ hydrocarbon$ at moment *t* was given as formula (S3):

$$C_i\ hydrocarbon_{sel}(\%) = \frac{moles\ of\ Ci\ \ hydrocarbon\ \times i}{m \times TOC} \times 100\% \quad \text{(S3)}$$

CO_2 selectivity (CO_{2sel}) was calculated by formula (S4):

$$CO_{2sel}(\%) = \frac{CO_{2t}}{CO_0 - CO_t} \times 100\% \quad \text{(S4)}$$

Where CO_{2t} denotes the moles of CO_2 at moment *t*.

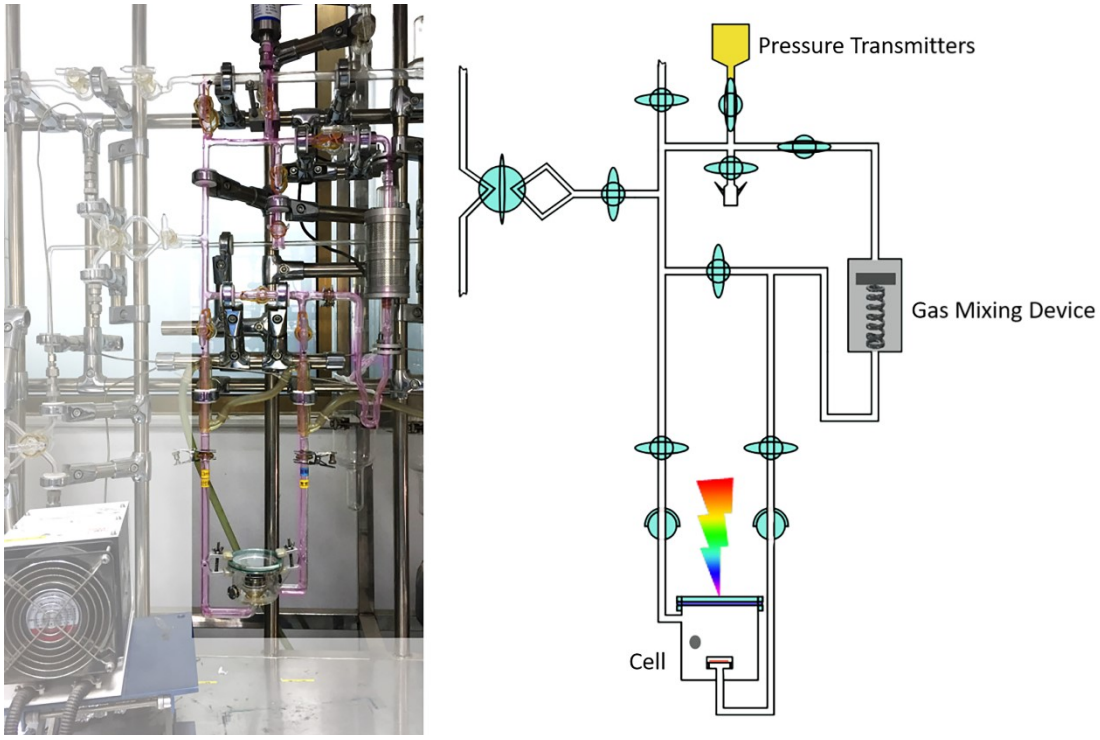

Fig. S1. The photograph and illustrated scheme of the enclosed-circuit system for catalyst performance test.

Table S1. Catalytic performance comparison.

Samples	CO_{con} (%)	selectivity (%)[a]			O/P	P (MPa)	T	Ref.
		CH_4	$C_{2=}$-$C_{4=}$	C_{2-}-C_{4-}				
Thermal Catalysis								
Fe-Zn-0.36Na	82.7	11.7	22.9	3.6	6.3	2.0	340 °C	[1]
Fe-Zn	34.1	27.1	13.3	16.6	0.8	2.0	340 °C	[1]
Fe-1.2Na	48.7	7.5	20.3	2.45	8.3	2.0	340 °C	[1]
Fe	32.7	21.0	17.5	10.9	1.6	2.0	340 °C	[1]
$ZnCrO_x$/MSAPO	17	2	80	14	5.7	2.5	400 °C	[2]
Photo+Thermal Catalysis								
30% Co/TNT	17.1	31.5	31.8	0.7	0.02	2.0	220 °C + UV light	[3]
Photothermal Catalysis								
Ni-500	14.9	30.6	33.0	32.1	1.0	0.18	300 W Xe lamp	[4]
3Co/STO	15.2	21.7	19.7	12.4	1.6	0.05	300 W Xe lamp	[5]
Co-450	15.4	48.0	36.0	5.9	6.1	0.18	300 W Xe lamp	[6]
CoMn alloys	13.9	28.4	27.0	8.4	3.22	0.18	300 W Xe lamp	[7]
α/γ-Fe_2O_3	28.8	24.8	71.9	4.06	16.7	0.05	300 W Xe lamp	This study

[a] $C_{2=}$-$C_{4=}$: olefins; C_{2-}-C_{4-}: paraffins;

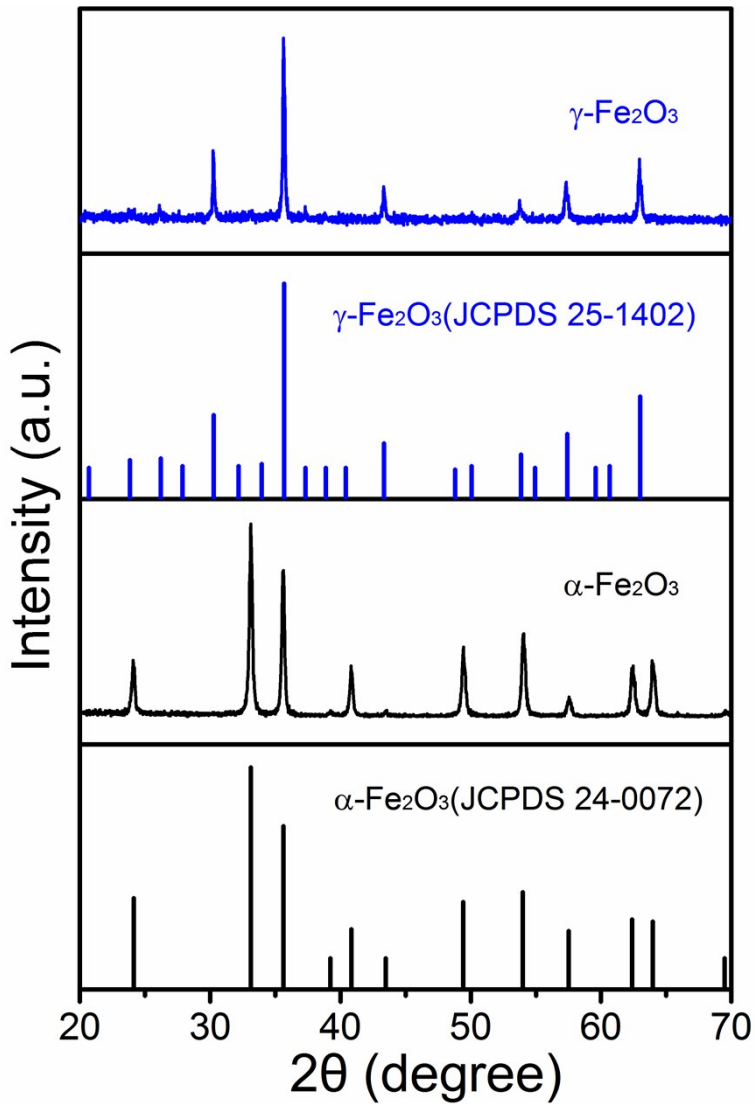

Fig. S2. The XRD pattern of Fe-based catalyst precursor α-Fe_2O_3 and γ-Fe_2O_3.

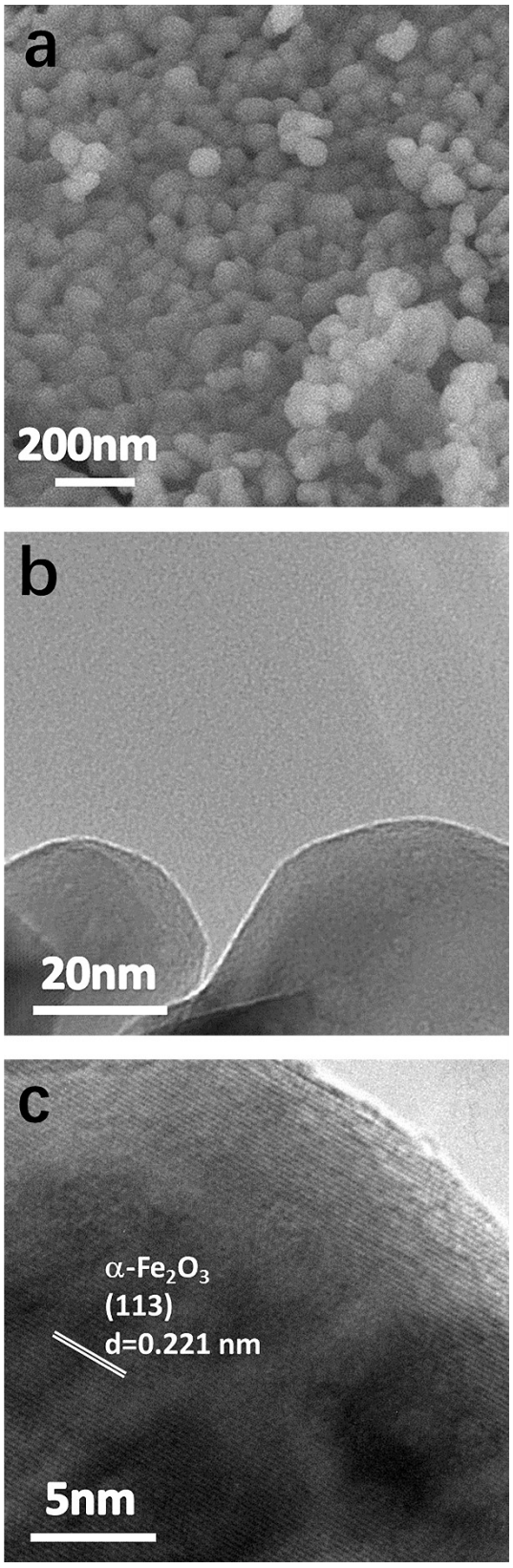

Fig. S3. a, SEM image, **b,** TEM image, **c,** HRTEM image of α-Fe_2O_3.

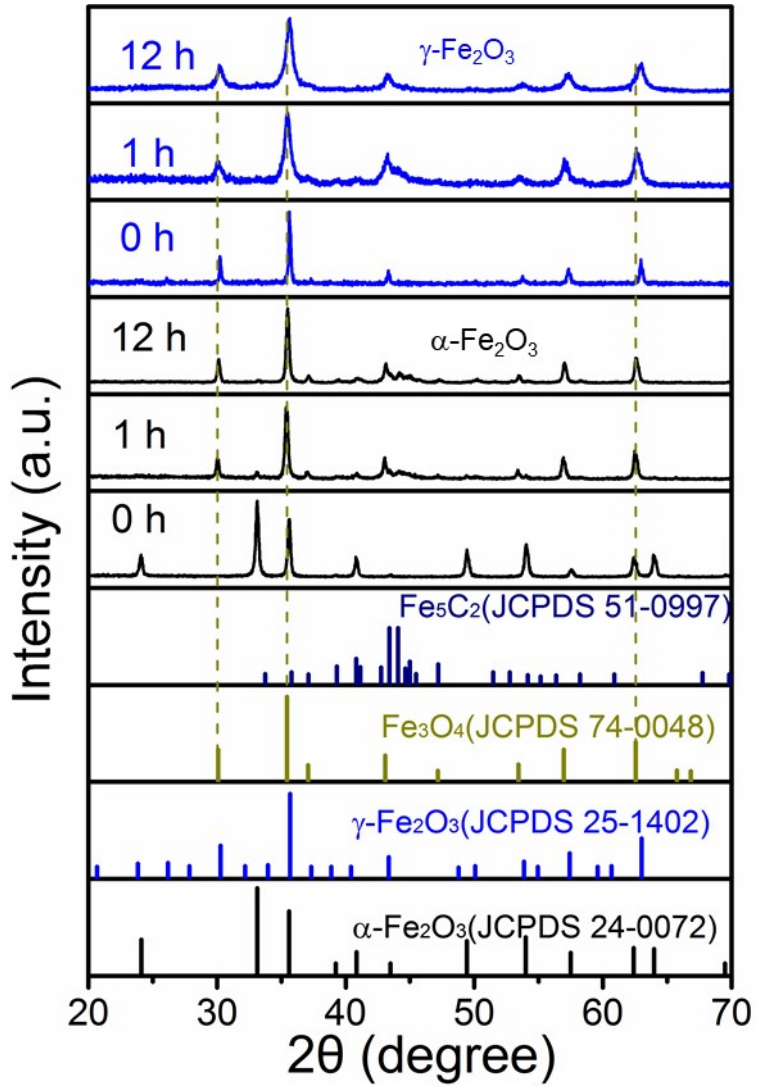

Fig. S4. The XRD pattern of α-Fe_2O_3 and γ-Fe_2O_3 before and after reaction.

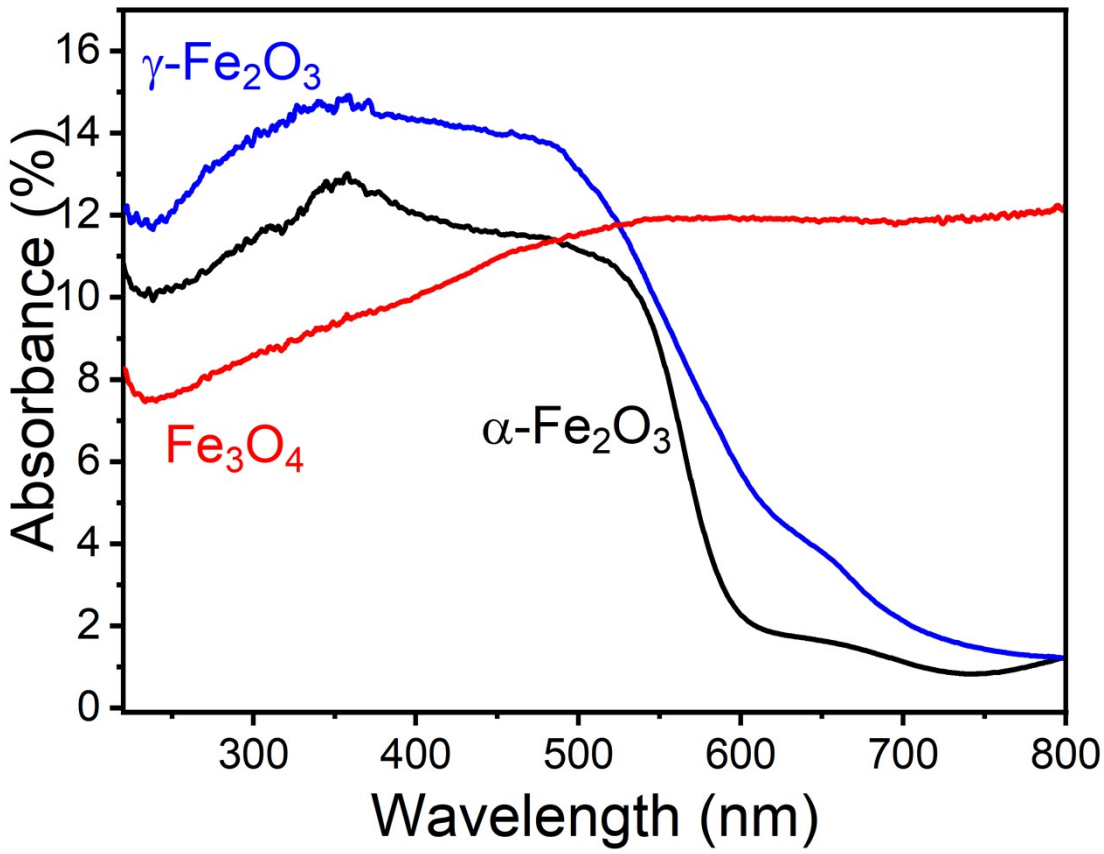

Fig. S5. UV-Vis spectra of α-Fe_2O_3 and γ-Fe_2O_3, and Fe_3O_4.

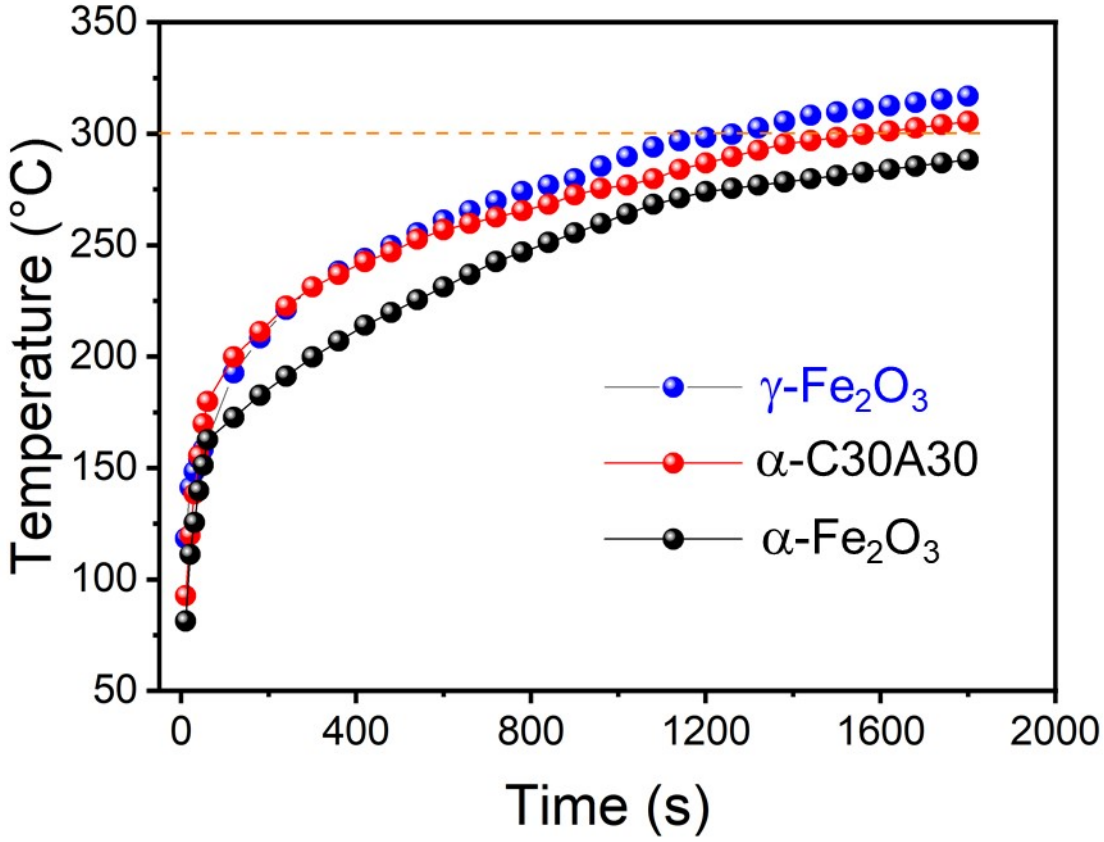

Fig. S6. Temperature variation curves of the catalysts during the reaction.

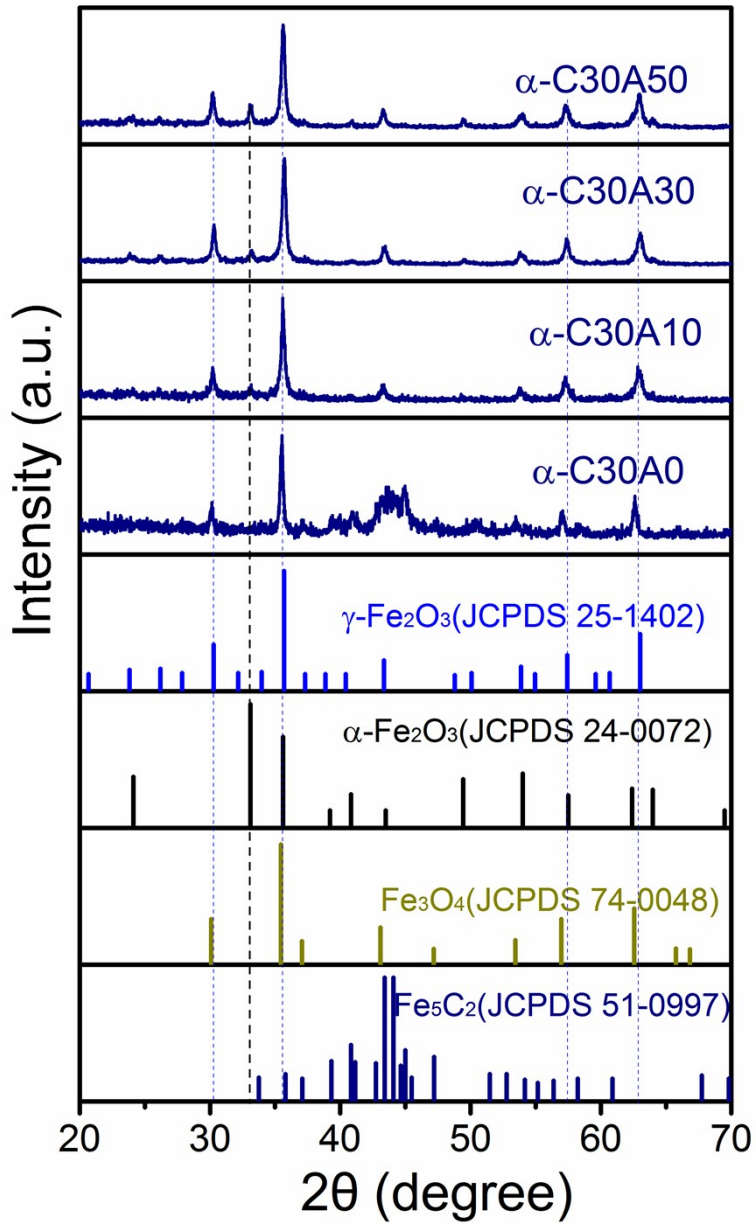

Fig. S7. The XRD pattern of photothermal synthesized composite catalyst precursor with α-Fe_2O_3 as the precursor.

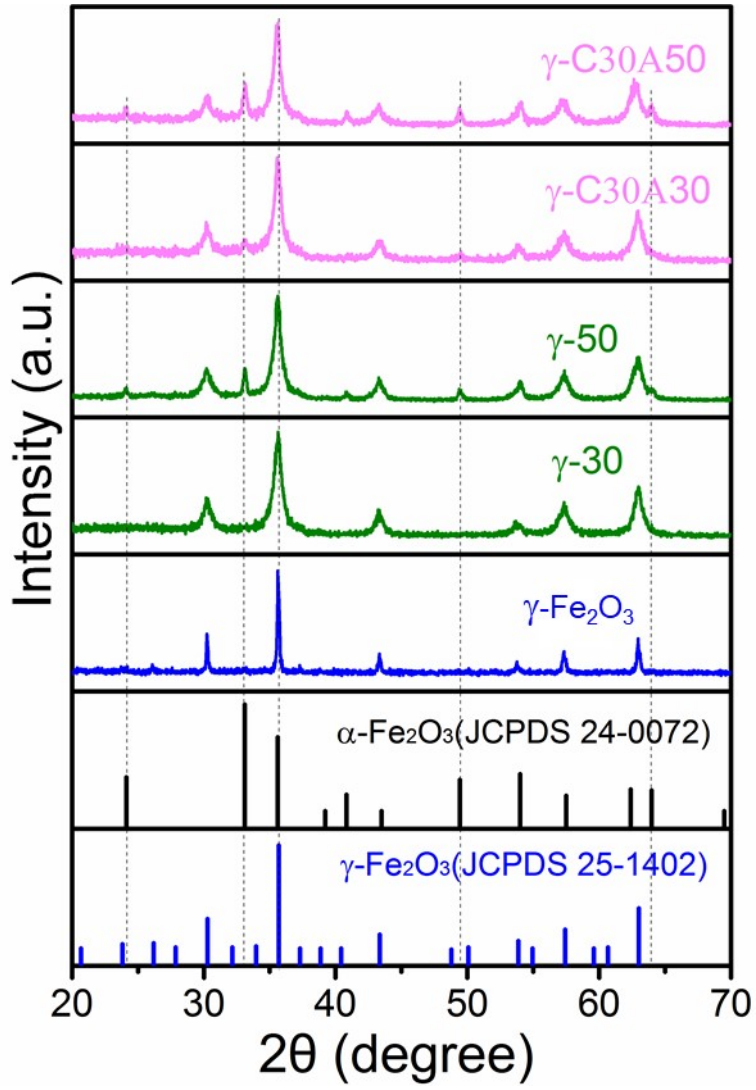

Fig. S8. The XRD pattern of photothermal synthesized composite catalyst precursor with γ-Fe_2O_3 as the precursor.

Table S2. Mössbauer parameters of α-C30A30.

Phase	Spectral Contribution(%)	IS (mms)	QS (mms)	Hhf (kOe)
α-Fe_2O_3	18.3	0.39	-0.21	514
γ-Fe_2O_3 (A)	50.7	0.35	---	483
γ-Fe_2O_3 (B)	31.0	0.30	0.06	500

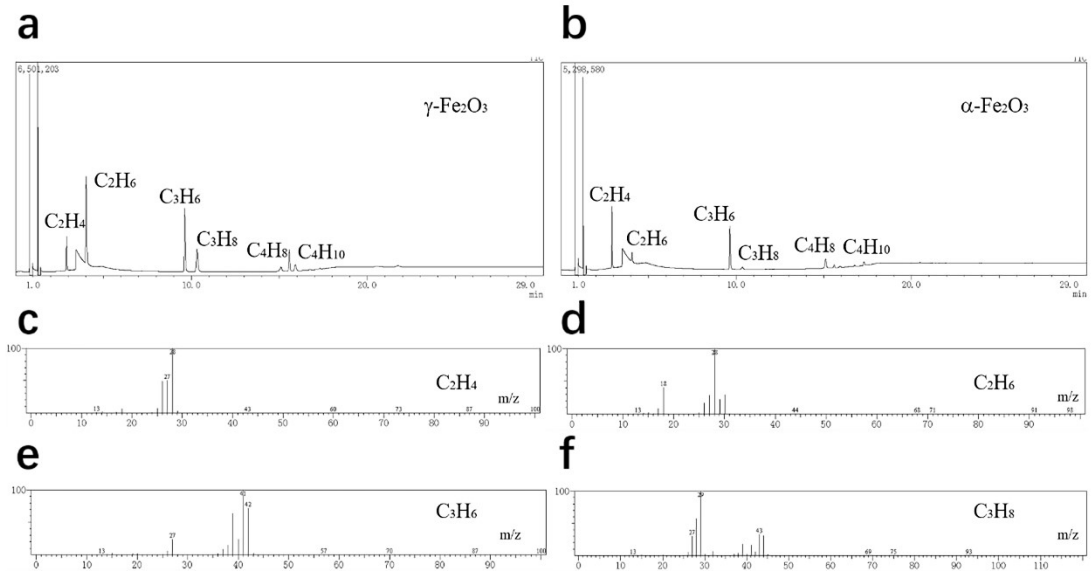

Fig. S9. The components of gas products of (a) α-Fe_2O_3 and (b) γ-Fe_2O_3, and Mass Spectrometry of (c) C_2H_4, (d) C_2H_6, (e) C_3H_6, and (f) C_3H_8.

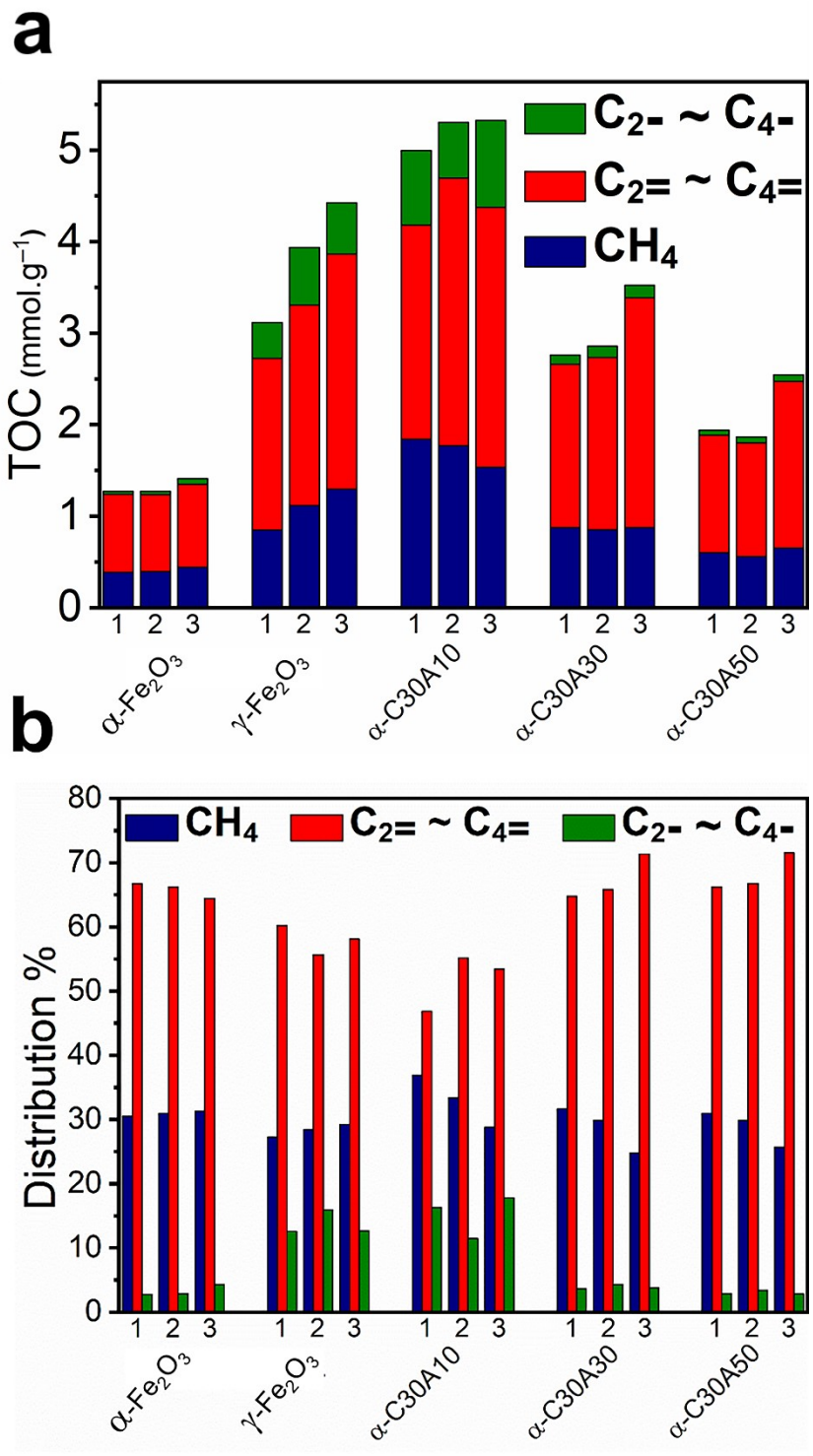

Fig. S10. The catalytic (a) activity and (b) selectivity of repeat experiments.

Table S3. The catalytic activity and selectivity.

Sample	CO_{Con} (%)	Selectivity (%)								TOC ($mmol.g^{-1}$)
		CH_4	$C_{2=}$	C_2	$C_{3=}$	C_3	$C_{4=}$	$C_2^{=}$-$C_4^{=}$	CO_2	
α-Fe_2O_3	11.8	31.3	33.3	36.5	24.5	25.6	6.6	64.4	75.8	1.4
γ-Fe_2O_3	24.0	28.4	22.7	34.3	28.0	32.4	4.9	55.6	66.8	3.9
α-C30A10	26.0	33.4	23.9	32.6	26.0	28.7	5.4	55.3	58.7	5.3
α-C30A30	28.8	24.8	32.1	34.7	27.9	29.1	11.9	71.9	75.2	3.5
α-C30A50	24.7	25.6	34.1	35.9	25.9	27.0	11.5	71.5	79.1	2.5

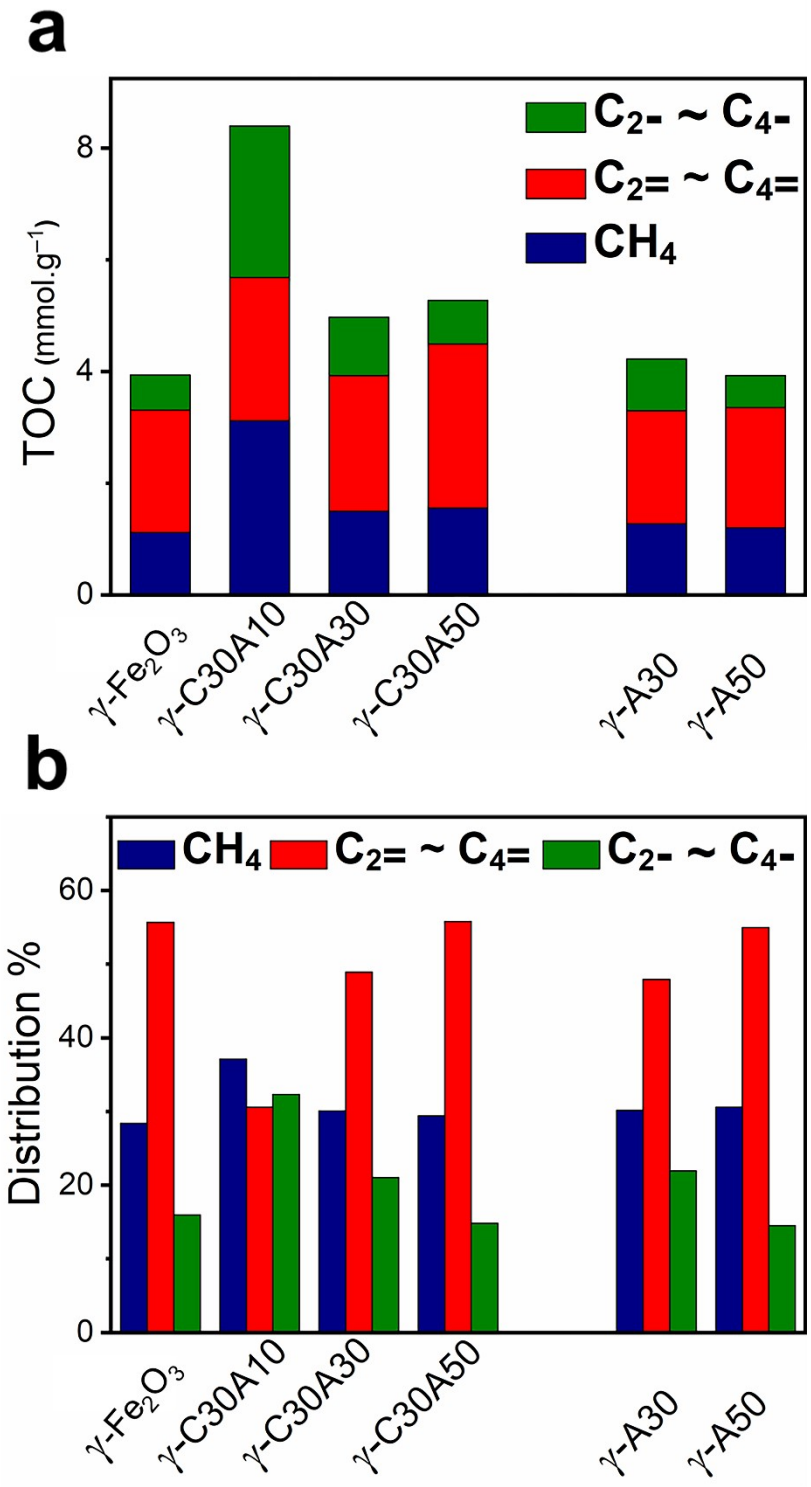

Fig. S11. The catalytic (a) activity and (b) selectivity of photothermal synthesized composite catalyst precursor with γ-Fe_2O_3 as the precursor.

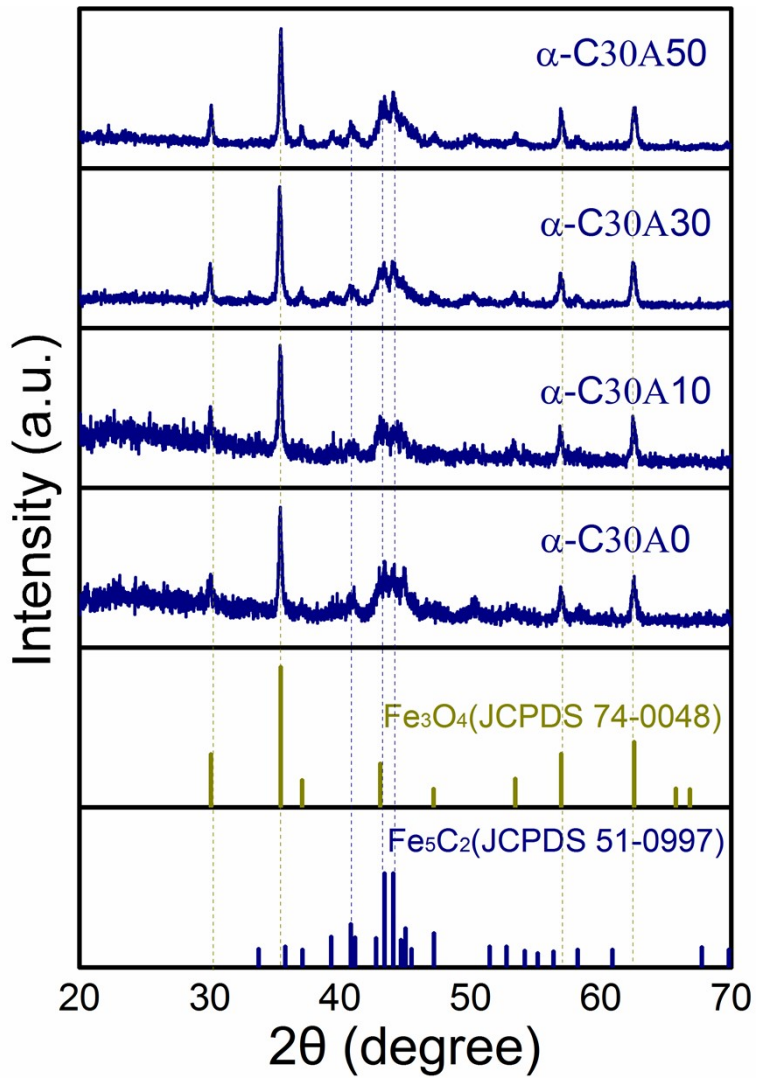

Fig. S12. The XRD pattern of catalysts after reaction.

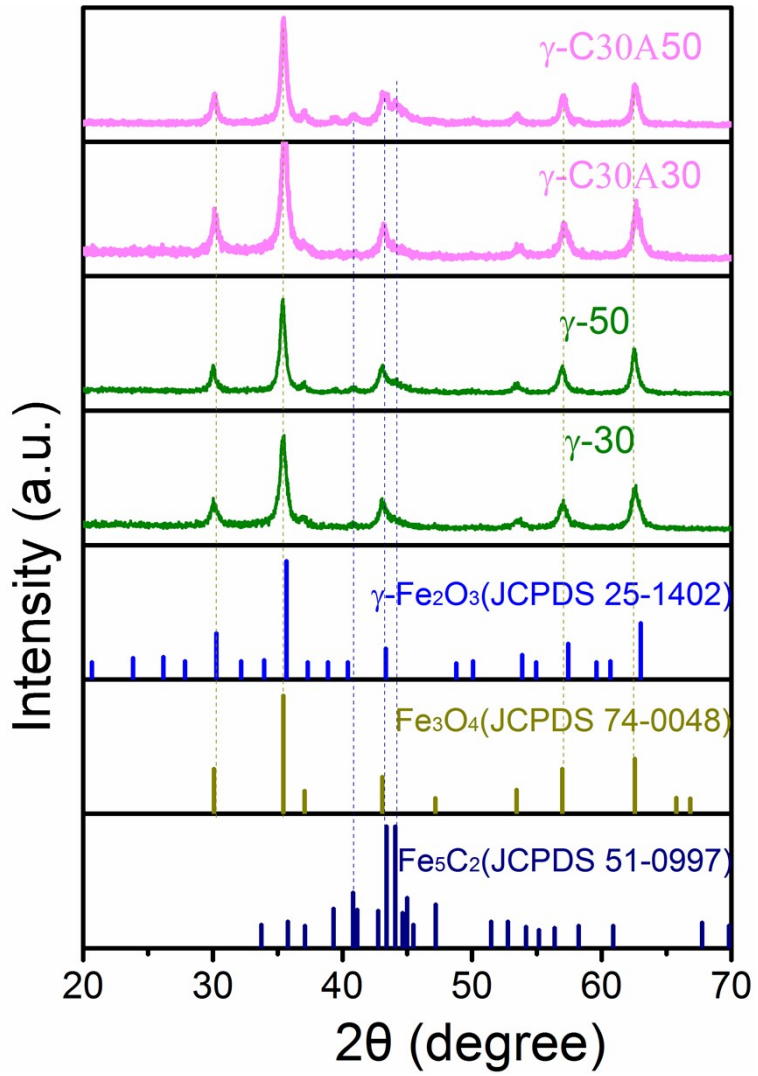

Fig. S13. The XRD pattern of catalysts after reaction.

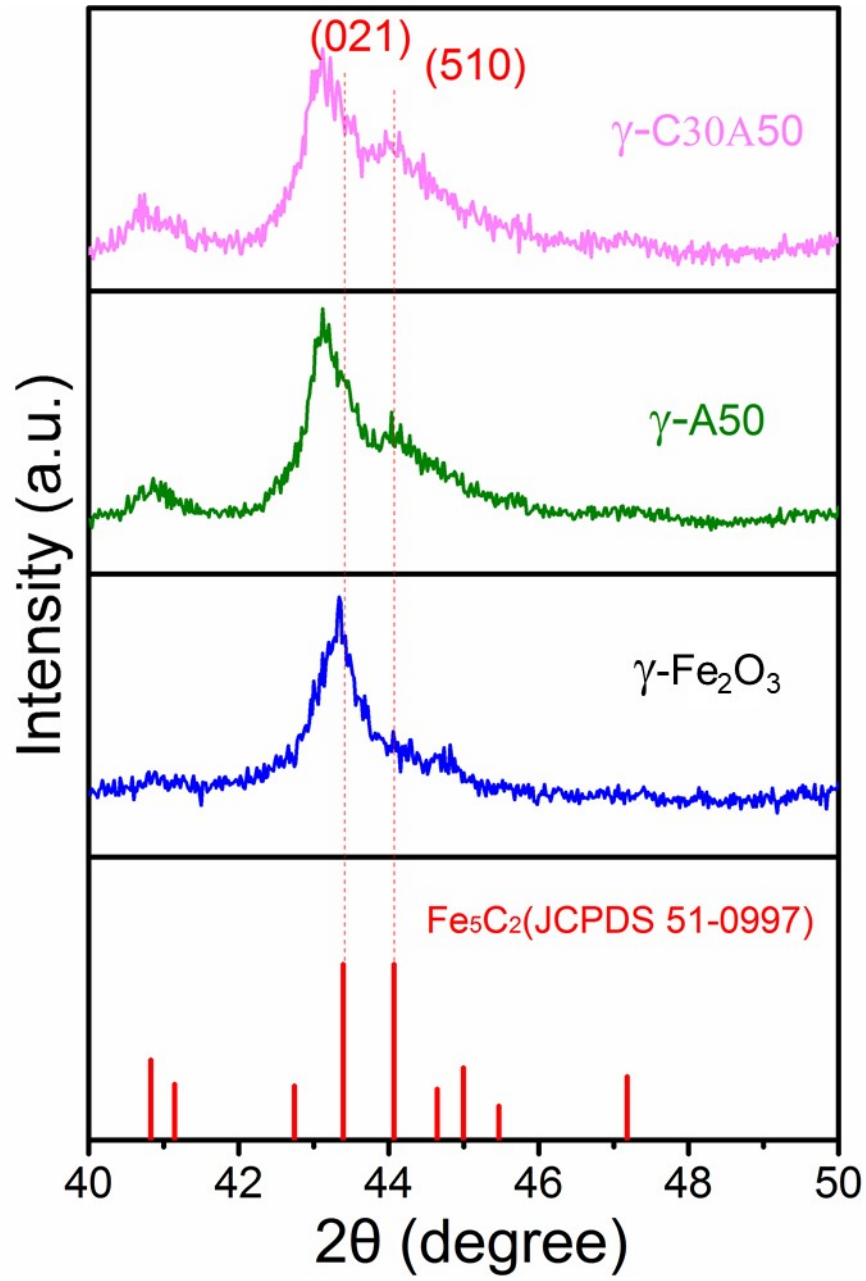

Fig. S14. The XRD pattern of catalysts after reaction.

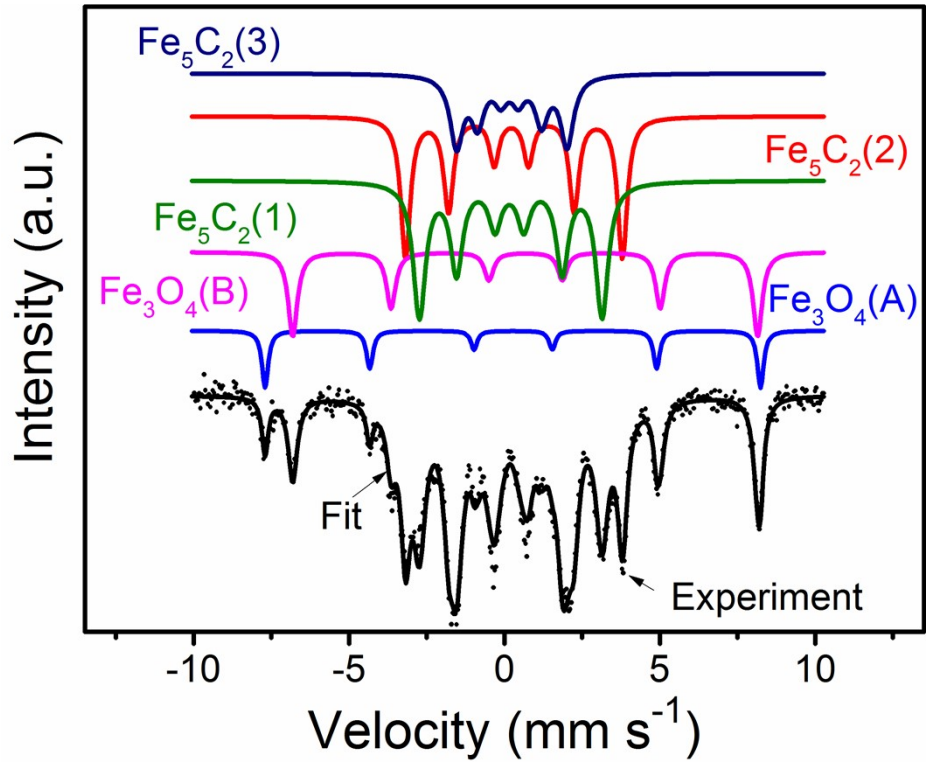

Fig. S15. Mössbauer spectra of α-C30A30 after reaction.

Table S4. Mössbauer parameters of α-C30A30 after reaction.

Phase	Spectral Contribution(%)	IS (mms)	QS (mms)	Hhf (kOe)
Fe_3O_4 (A)	7.0	0.28	-0.01	496
Fe_3O_4 (B)	15.2	0.68	-0.01	465
Fe_5C_2 (1)	32.9	0.18	0.04	182
Fe_5C_2 (2)	26.7	0.27	0.09	217
Fe_5C_2 (3)	18.1	0.20	0.07	111

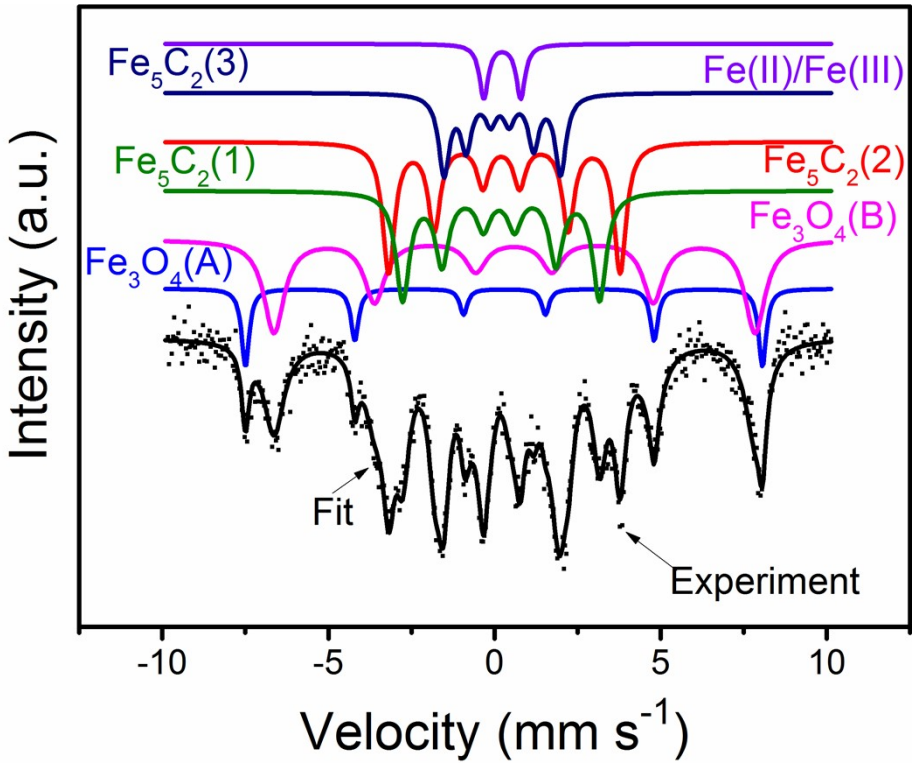

Fig. S16. Mössbauer spectra of γ-Fe_2O_3 after reaction.

Table S5. Mössbauer parameters of γ-Fe_2O_3 after reaction.

Phase	Spectral Contribution(%)	IS (mms)	QS (mms)	Hhf (kOe)
Fe_3O_4 (A)	9.0	0.29	-0.02	484
Fe_3O_4 (B)	28.5	0.59	-0.01	450
Fe_5C_2 (1)	22.1	0.17	0.06	184
Fe_5C_2 (2)	23.8	0.25	0.10	216
Fe_5C_2 (3)	13.0	0.20	0.07	109
Fe(II)Fe(III)	3.6	0.23	1.11	---

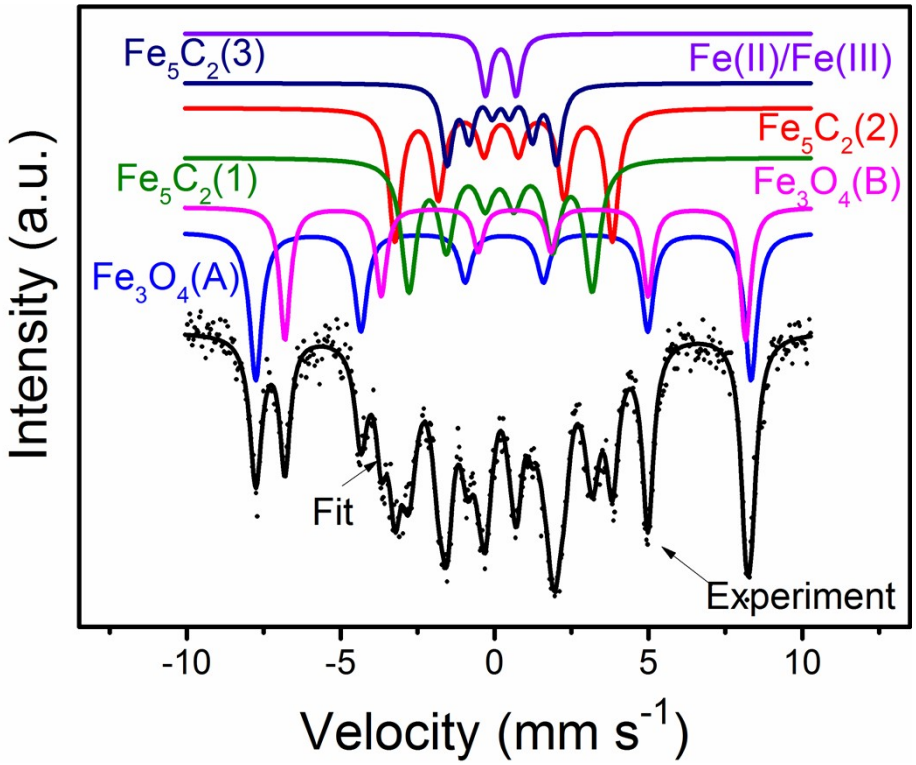

Fig. S17. Mössbauer spectra of α-Fe_2O_3 after reaction.

Table S6. Mössbauer parameters of α-Fe_2O_3 after reaction.

Phase	Spectral Contribution(%)	IS (mms)	QS (mms)	Hhf (kOe)
Fe_3O_4 (A)	22.8	0.30	0.03	500
Fe_3O_4 (B)	17.5	0.67	0.02	465
Fe_5C_2 (1)	24.7	0.18	0.03	185
Fe_5C_2 (2)	20.3	0.26	0.08	220
Fe_5C_2 (3)	10.9	0.21	0.04	111
Fe(II)Fe(III)	3.8	0.21	1.00	---

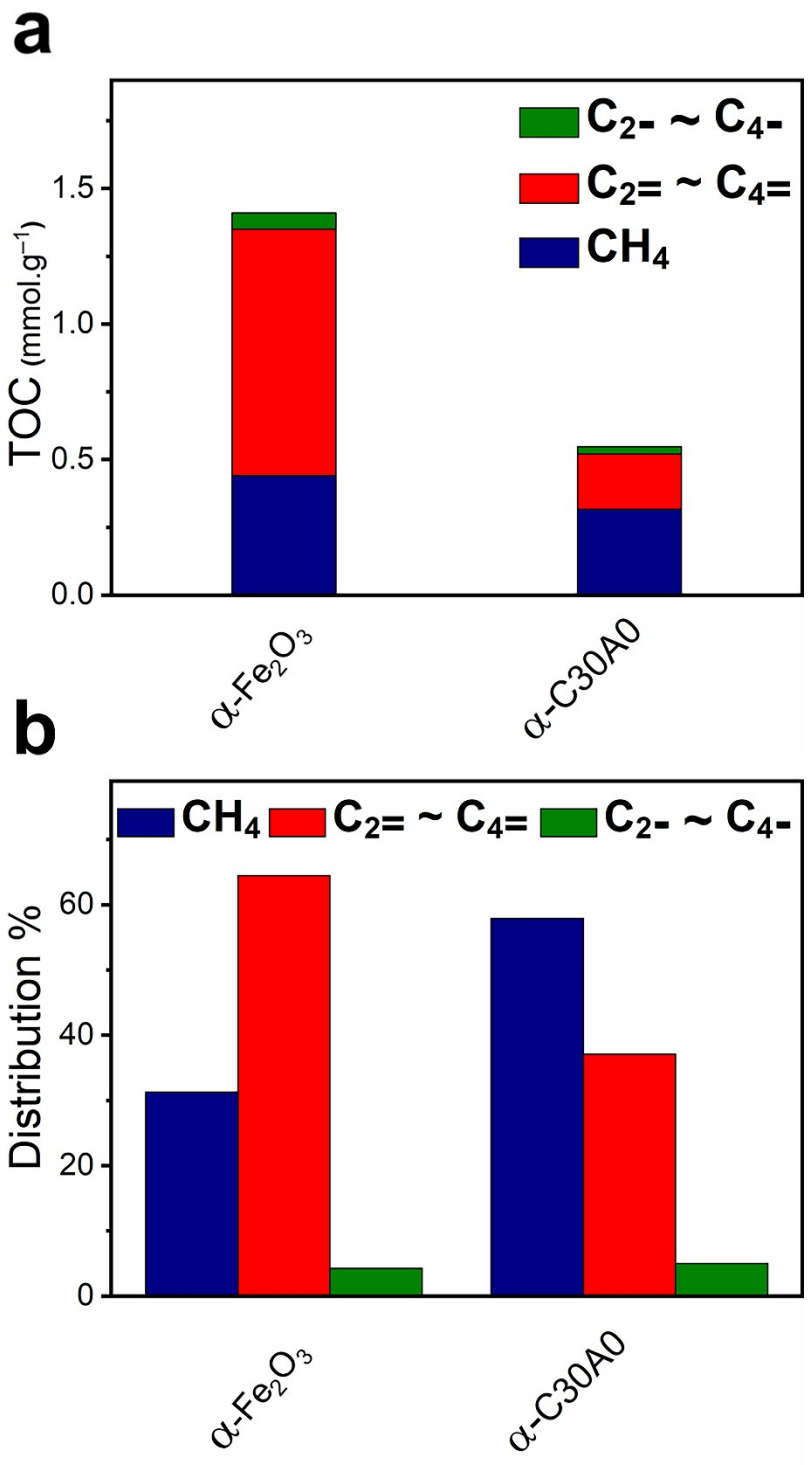

Fig. S18. The catalytic (a) activity and (b) selectivity of α-Fe_2O_3 and α-C30A30.

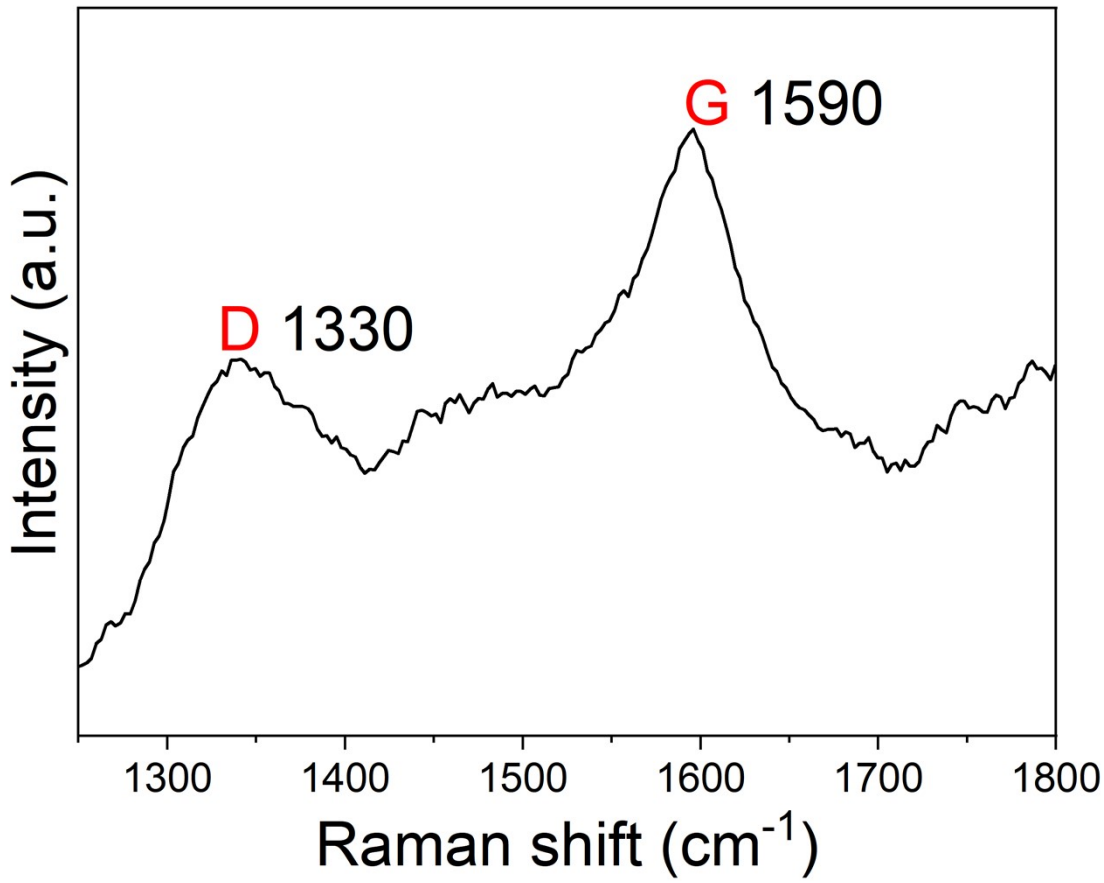

Fig. S19. Raman spectra of α-C30A0.

Theoretical Calculation

The DFT calculations were carried out by using the Vienna ab initio simulation package (VASP)[8, 9]. The exchange-correlation interaction is described by generalized gradient approximation (GGA) with the Perdew–Burke–Ernzerhof (PBE) functional[10]. The Van der Waals interaction was described by using the empirical correction in Grimme's scheme, i.e. DFT+D_3[11]. The energy cutoff was set to 500 eV. To model (021) surface, a 3-atom-layer slab, including two buffer layers and one fixed layer, were used. For (510) surface's case, a slab with two buffer layers and two fixed layers were constructed. In addition, a vacuum region of 15 Å was used to avoid the interactions among the periodic slabs. The CO_2 reduction was processed on the top of (510) and (021) surfaces (vacuum region). The Brillouin zone was sampled by a Monkhorst-Pack 2 × 3 × 1 and 3 × 2 × 1 K-point grid in reciprocal space for (510) and (021) slabs, respectively. The CI-NEB method was used to find saddle points and minimum energy paths[12]. In all of our calculations, atoms in fixed region are held fixed at the bulk positions, while the atoms in the buffer and vacuum regions are fully relaxed until all force components acting on the atoms are below 0.005 eV/Å.

Table S7. Influence of crystal facet on CH_4 formation reaction barrier and reaction energy.

Reactions		(021)				(510)		
	Total energy (eV)		Ea (eV)	△E (eV)	Total energy (eV)		Ea (eV)	△E (eV)
C+H ↓ CH	R	-919.96	1.00	0.35	R	-682.43	0.80	0.53
	TS	-918.96			TS	-681.63		
	P	-919.61			P	-681.90		
CH+H ↓ CH_2	R	-923.69	1.04	0.90	R	-685.98	0.96	0.83
	TS	-922.65			TS	-685.02		
	P	-922.79			P	-685.15		
CH_2+H ↓ CH_3	R	-926.84	0.97	0.18	R	-689.20	0.67	0.37
	TS	-925.87			TS	-688.52		
	P	-926.66			P	-688.82		
CH_3+H ↓ CH_4	R	-930.75	1.15	0.24	R	-692.91	1.45	0.46
	TS	-929.60			TS	-691.46		
	P	-930.51			P	-692.46		

Table S8. Influence of crystal facet on C-C coupling reaction barrier and reaction energy.

Reactions	(021)				(510)			
	Total energy (eV)		Ea (eV)	△E (eV)	Total energy (eV)		Ea (eV)	△E (eV)
CH_2+CH_2 ↓ CH_2CH_2	R	-930.41	1.05	-0.17	R	-701.90	1.07	0.17
	TS	-929.36			TS	-700.83		
	P	-930.57			P	-701.73		
CH_2CH_2+H ↓ CH_2CH_3	R	-934.62	0.39	0.26	R	-705.89	1.00	0.66
	TS	-934.24			TS	-704.89		
	P	-934.37			P	-705.24		
CH_2CH_3+H ↓ CH_3CH_3	R	-938.41	1.32	0.43	R	-709.38	1.00	0.36
	TS	-937.08			TS	-708.38		
	P	-937.98			P	-709.03		
CH_2+CH_2CH_2 ↓ $CH_2CH_2CH_2$	R	-947.21	0.84	-0.13	R	-718.91	1.98	0.84
	TS	-946.37			TS	-716.94		
	P	-947.35			P	-718.08		
$CH_2CH_2CH_2$ ↓ CH_2CHCH_2+H	R	-947.35	1.02	-0.84	R	-718.08	0.24	-0.75
	TS	-946.33			TS	-717.84		
	P	-948.18			P	-718.83		
CH_2CHCH_2+H ↓ CH_2CHCH_3	R	-948.18	1.17	0.81	R	-718.83	0.94	0.25
	TS	-947.02			TS	-717.89		
	P	-947.37			P	-718.58		
$CH_2CH_2CH_2$+H ↓ $CH_2CH_2CH_3$	R	-951.22	0.94	0.26	R	-721.99	1.00	-0.18
	TS	-950.28			TS	-720.98		
	P	-950.95			P	-722.16		
$CH_2CH_2CH_3$+H ↓ $CH_3CH_2CH_3$	R	-955.06	1.37	0.46	R	-726.41	1.83	0.65
	TS	-953.69			TS	-724.59		
	P	-954.60			P	-725.76		
CH_3CHCH_2+H ↓ $CH_3CH_2CH_2$	R	-951.39	2.05	0.43	R	-722.75	1.23	0.59
	TS	-949.34			TS	-721.52		
	P	-950.95			P	-722.16		
$CH_2CH_2CH_3$+H ↓ $CH_3CH_2CH_3$	R	-955.06	1.37	0.46	R	-726.41	1.83	0.65
	TS	-953.69			TS	-724.59		
	P	-954.60			P	-725.76		
CH_2+$CH_2CH_2CH_2$ ↓ $CH_2CH_2CH_2CH_2$	R	-963.90	1.60	-0.06	R	-725.61	2.88	1.21
	TS	-962.30			TS	-722.73		
	P	-963.96			P	-724.41		

References

1. P. Zhai, C. Xu, R. Gao, X. Liu, M. Li, W. Li, X. Fu, C. Jia, J. Xie, M. Zhao, X. Wang, Y.-W. Li, Q. Zhang, X.-D. Wen and D. Ma, *Angewandte Chemie International Edition*, 2016, **55**, 9902-9907.
2. F. Jiao, J. Li, X. Pan, J. Xiao, H. Li, H. Ma, M. Wei, Y. Pan, Z. Zhou, M. Li, S. Miao, J. Li, Y. Zhu, D. Xiao, T. He, J. Yang, F. Qi, Q. Fu and X. Bao, *Science*, 2016, **351**, 1065-1068.
3. L. Wang, Y. Zhang, X. Gu, Y. Zhang and H. Su, *Catalysis Science & Technology*, 2018, **8**, 601-610.
4. Y. Wang, Y. Zhao, J. Liu, Z. Li, G. I. N. Waterhouse, R. Shi, X. Wen and T. Zhang, *Advanced Energy Materials*, 2020, **10**, 1902860.
5. S. Ning, S. Wang, S. Ouyang, Y. Qi, X. Yi, H. Hu and J. Ye, *Catalysis Science & Technology*, 2021, **11**, 7029-7034.
6. Z. Li, J. Liu, Y. Zhao, G. I. N. Waterhouse, G. Chen, R. Shi, X. Zhang, X. Liu, Y. Wei, X.-D. Wen, L.-Z. Wu, C.-H. Tung and T. Zhang, *Advanced Materials*, 2018, **30**, 1800527.
7. R. Li, Y. Li, Z. Li, W. Wei, S. Ouyang, H. Yuan and T. Zhang, *Solar RRL*, 2021, **5**, 2000488.
8. G. Kresse and J. Furthmüller, *Phys. Rev. B*, 1996, **54**, 11169-11186.
9. G. Kresse and J. Furthmüller, *Comput. Mater. Sci.*, 1996, **6**, 15-50.
10. J. P. Perdew, K. Burke and M. Ernzerhof, *Phys. Rev. Lett.*, 1996, **77**, 3865-3868.
11. S. Grimme, *J. Comput. Chem.*, 2006, **27**, 1787-1799.
12. G. Henkelman, B. P. Uberuaga and H. Jónsson, *J. Chem. Phys.*, 2000, **113**, 9901-9904.